

# Multi-tone Signal Optimization for Wireless Power Transfer in the Presence of Wireless Communication Links

Boules A. Mouris, *Student Member, IEEE*, Hadi Ghauch, *Member, IEEE*,  
Ragnar Thobaben, *Member, IEEE*, and B. L. G. Jonsson

## Abstract

In this paper, we study optimization of multi-tone signals for wireless power transfer (WPT) systems. We investigate different non-linear energy harvesting models. Two of them are adopted to optimize the multi-tone signal according to the channel state information available at the transmitter. We show that a second-order polynomial curve-fitting model can be utilized to optimize the multi-tone signal for any RF energy harvester design. We consider both single-antenna and multi-antenna WPT systems. In-band co-existing communication links are also considered in this work by imposing a constraint on the received power at the nearby information receiver to prevent its RF front end from saturation. We emphasize the importance of imposing such constraint by explaining how inter-modulation products, due to saturation, can cause high interference at the information receiver in the case of multi-tone signals. The multi-tone optimization problem is formulated as a non-convex linearly constrained quadratic program. Two globally optimal solution approaches using mixed-integer linear programming and finite branch-and-bound techniques are proposed to solve the problem. The achieved improvement resulting from applying both solution methods to the multi-tone optimization problem is highlighted through simulations and comparisons with other solutions existing in the literature.

## Index Terms

Wireless power transfer, non-linear energy harvester, multi-tone optimization.

B. A. Mouris, R. Thobaben and B. L. G. Jonsson are with the School of Electrical Engineering and Computer Science (EECS), KTH Royal Institute of Technology, Stockholm 100 44, Sweden (e-mail:boules@kth.se).

H. Ghauch is with the Department of COMELEC, Telecom-ParisTech, Institut Mines-Telecom, Paris, France (e-mail:hadi.ghauch@telecom-paristech.fr).

## I. INTRODUCTION

The massive increase in the number of wireless devices in future communication systems such as Internet of Things (IoT) and fifth-generation (5G) networks has increased the demand to eliminate wires completely from electronics devices [1]. Wireless power transfer (WPT) is a promising way to cross the barrier imposed by batteries. The history of wireless power transfer dates back to the Tesla coil more than 100 years ago. However, with recent advancements in microwave technology and antenna design, extensive research addressing WPT technology has been conducted over the last decade [2], [3]. In order to fully power electronic devices wirelessly, two research directions have been investigated: minimizing power consumption in electronic devices, and improving WPT efficiency. Recently, energy-efficient wireless sensors were proposed in [4], in which analog joint source-channel coding was exploited to compress sensor signals allowing a power consumption as low as  $90 \mu\text{W}$ . Such sensors can be fully operated by wireless power, and thus, enable autonomous wireless sensor networks.

In the context of limiting battery usage in communication systems, extensive research has been devoted to studying wireless powered communications (WPC) [5] as well as simultaneous wireless information and power transfer (SWIPT) [6]. An example for WPC is [7], where wireless power transfer is used to enable load modulated backscatter communication. Resource allocation for different SWIPT techniques in broadband systems has been discussed in [8]. The rate-energy region for different SWIPT schemes has been characterized in [9]. However, these contributions assumed a linear energy harvester model, in which the output power is a linear function of the input power to the energy harvester. More recently, different non-linear energy harvester models have been proposed to model the performance of SWIPT systems more specifically [10]–[12]. These models will be discussed in more details in Section III in this paper.

The key element of a WPT system is the RF energy harvester which is responsible for capturing the incident electromagnetic wave and converting it efficiently into DC power. The RF-to-DC conversion efficiency of the RF energy harvester, usually referred to as rectenna (rectifying antenna), determines the overall efficiency of the WPT system. Designing an efficient rectenna is a major challenge, especially at very low input RF power levels. Many research efforts have been directed towards improving the efficiency of rectennas by carefully designing its components as in [13]–[16]. In [13], a dual-polarized antenna followed by two voltage doubler circuits were proposed to combine RF power arriving from different polarizations. An adaptive re-configurable

rectifier that maintains its efficiency with respect to the input power level was presented in [14]. Different configurations of rectenna arrays were investigated to increase the output DC power in [15]. A broadband rectenna with a highly efficient rectifier circuit was proposed in [16].

Lately, it has been observed experimentally that signals having high peak-to-average power ratio (PAPR) such as chaotic, white noise and OFDM signals [17] can boost the RF-to-DC conversion efficiency of RF energy harvesters. Multisine signals having high PAPR were shown to improve the range and reliability of RFID tag systems in [18]. These interesting results motivated research on analyzing the dependency of the efficiency of the energy harvester on its input waveform [18], [19]. However, these studies ignored the wireless channel in their analysis. To the authors best knowledge, [20] was the first work to account for the wireless channel and the channel state information (CSI) available at the transmitter in addition to the non-linear behavior of the energy harvester in designing the WPT signal. A model based on Taylor expansion of the I-V characteristics of the diode has been adopted in [20] and used for waveform design showing performance gains over linear models when exploiting multi-tone signal excitation. In [21], a similar work has been proposed using the I-V characteristics of the diode utilizing integral equations instead of the Taylor expansion. In both [20], [21], the weights (amplitudes and phases) of the multi-tone signal resulting from maximizing the output DC current from the energy harvester subject to a transmit power constraint were obtained. The globally optimal phases were obtained in closed form, although the amplitudes were not guaranteed to be globally optimal.

In this paper, we introduce a globally optimal solution method to the multi-tone signal optimization problem to obtain the amplitudes of the multi-tone signal. We first use the diode non-linear model to express the output DC current from the energy harvester. However, in contrast to [20], [21], we formulate the output maximization problem as linearly constrained quadratic program (LCQP), for which we introduce two globally optimal solution methods using either mixed-integer linear programming (MILP) or finite branch-and-bound (BB). Secondly, we introduce a simple second-order polynomial curve-fitting model with the same goal of designing the amplitudes and phases of the multi-tone signals. We show by designing and simulating a 2.4 GHz energy harvester that the curve-fitting model tends to show the same behavior for power allocation as the diode model. We also consider the problem of multi-tone signal optimization in a MISO WPT system. Finally, assuming in-band SWIPT, we consider preserving the information link between co-existing communication devices by adding a constraint on the received power

at the nearby information receiver to keep it below the saturation point of its low-noise amplifier (LNA). This constraint was motivated by a practical experiment conducted by the authors: A Wi-Fi channel between a router and a computer was established (channel 7 in IEEE 802.11g). By implementing multi-tone signal WPT with software defined radios at 2.4 GHz, a significant decrease in the rate of information transfer (compared to single-tone WPT) has been observed, even when the multi-tone signals are designed to not interfere with any OFDM sub-carrier. The authors explained this by taking into account the RF front-end of the information receiver (before mixing and converting to base-band), hence, adding a constraint preventing the LNA from producing high-order harmonics.

The contributions of this work can be summarized as follows: We formulate the multi-tone optimization problem resulting from the Taylor expansion of the I-V characteristics of the diode as a LCQP and propose two globally optimal solution methods to obtain the amplitudes of the multi-tone signal. Simulation results show that applying the proposed solution methods to the multi-tone optimization problem enhances the output of the energy harvester compared to the other power allocation methods existing in the literature. We explain how a second-order polynomial curve-fitting model can be utilized in the multi-tone signal optimization problem. Our simulation results show excellent agreement between the diode model and the curve-fitting model. The advantage of using this curve-fitting model arises from the fact that it can easily be adjusted in the case of multi-stage rectifiers to simplify the formulation of the multi-tone optimization problem. We also investigate the problem of in-band SWIPT from a practical aspect by considering the RF front end of the information receiver. Our simulation results confirms the importance of considering the saturation power as well as the distance of the nearby information receiver from the power transmitter when using multi-tone signals for WPT. The rest of the paper is organized as follows: Section II introduces the system model and Section III discusses different non-linear energy harvester models. Section IV presents the formulation and the proposed solution methods for the multi-tone optimization problem resulting from the adopted two non-linear energy harvesting models. The problem of in-band SWIPT is discussed in Section V. The simulations results are shown in Section VI. Section VII concludes the paper and discusses possible future work.

*Notation:* Matrices and vectors are represented by bold upper and lower case letters, respectively. Non-bold symbols represent scalars. The Euclidean norm is represented by  $\|\mathbf{x}\| = \sqrt{|x_1|^2 + \dots + |x_n|^2}$ .  $\mathbb{E}\{\cdot\}$  denotes the expectation. We refer to the real part of a complex

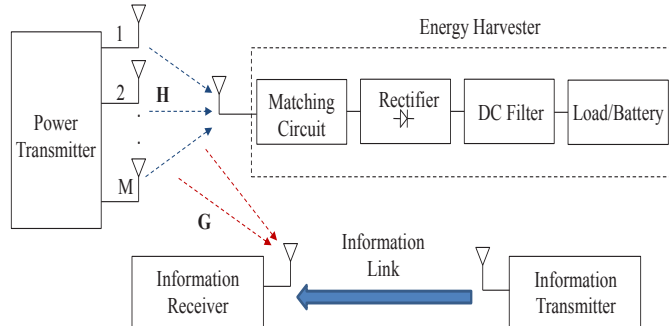


Fig. 1. Co-existing Wireless Power and Information Transfer.

quantity by  $\Re\{\cdot\}$ .  $\mathbf{X}^T$  and  $\mathbf{X}^H$  refer to the transpose and conjugate transpose of a matrix, respectively.  $\text{tr}(\mathbf{X})$  represents the trace of a matrix. We let  $\mathcal{CN}(\mu, \sigma^2)$  be a complex Gaussian random variable with mean  $\mu$  and variance  $\sigma^2$ .

## II. SYSTEM MODEL

In this paper, we study the scenario presented in Fig. 1, in which a wireless power transmitter sends power to an energy harvester in the vicinity of an information receiver which is communicating with an information transmitter using an OFDM-based radio access technology. It should be noted that in our analysis, we consider interference-unaware OFDM-based radio communication. This means that the information transmitter and receiver are not aware of the possible interference caused by the power transmitter. Such a scenario is prone to happen in an era of IoT where some devices or sensors are receiving wireless power in the vicinity of a Wi-Fi router that is communicating with smart phones or laptop computers. The power transmitter is equipped with  $M$  antennas, while the energy harvester, the information transmitter, and the information receiver are equipped with a single antenna for each.

We assume that the power transmitter is transmitting  $N$  tones with frequencies  $f_n$  such that  $f_n = f_o + (n - 1) \Delta f_p$  where  $\Delta f_p$  is the sub-carrier spacing for the multi-tone signal for WPT and  $f_o$  is the carrier frequency. The transmitted WPT signal at the  $m^{\text{th}}$  antenna is given by

$$x_{P,m}(t) = \sum_{n=1}^N s_{n,m} \cos(2\pi f_n t + \phi_{n,m}) = \Re \left\{ \sum_{n=1}^N s_{n,m} e^{j2\pi f_n t} e^{j\phi_{n,m}} \right\}, \quad (1)$$

with  $s_{n,m}$  and  $\phi_{n,m}$  referring to the amplitude and the phase of the  $n^{\text{th}}$  tone at antenna  $m$ , respectively. Let  $w_{n,m} = s_{n,m} e^{j\phi_{n,m}}$ ,  $\mathbf{w}_n = [w_{n,1}, w_{n,2}, \dots, w_{n,m}]^T$  and  $\mathbf{x}_p(t) = [x_{P,1}(t), x_{P,2}(t), \dots, x_{P,M}(t)]^T$ .

We can write the transmitted power signal as

$$\mathbf{x}_p(t) = \Re \left\{ \sum_{n=1}^N \mathbf{w}_n e^{j2\pi f_n t} \right\}. \quad (2)$$

The transmitted power signal is limited by a transmit power constraint given by  $\sum_{m=1}^M \mathbb{E} \{|x_{P,m}|\}^2 \triangleq \frac{1}{2} \|\mathbf{S}\|^2 \leq P$ , where the matrix  $\mathbf{S} = [s_{n,m}]$  contains the non-negative amplitudes of the multi-tone signal. The factor  $\frac{1}{2}$  is due to the sinusoidal nature of the multi-tone signal. The channel frequency response from the transmitter to the energy harvester at  $f_n$  can be described by the row vector  $\mathbf{h}_n = [h_{n,1}e^{j\psi_{n,1}}, h_{n,2}e^{j\psi_{n,2}}, \dots, h_{n,M}e^{j\psi_{n,M}}]$  where  $h_{n,m}e^{j\psi_{n,m}}$  represents the channel frequency response at the  $n^{\text{th}}$  tone of antenna  $m$ . The matrix  $\mathbf{H}$  shown in Fig. 1 contains all the row vectors  $\mathbf{h}_n$  for all tones.

At the energy harvester, the received signal can be written as

$$y_p(t) = \Re \left\{ \sum_{n=1}^N \mathbf{h}_n \mathbf{w}_n e^{j2\pi f_n t} \right\} + v(t), \quad (3)$$

where  $v$  is additive white Gaussian noise with variance  $\sigma^2$ . The noise power is assumed to be negligible compared to transmitted power, and therefore, we eliminate the noise from further analysis in this paper.

Assume that the frequency response of the channel from the power transmitter to the nearby information receiver is given by  $\mathbf{G}$  as shown in Fig. 1. The rows of  $\mathbf{G}$  represent the vector channel at the  $n^{\text{th}}$  tone given by  $\mathbf{g}_n = [g_{n,1}e^{j\zeta_{n,1}}, g_{n,2}e^{j\zeta_{n,2}}, \dots, g_{n,M}e^{j\zeta_{n,M}}]$  where  $g_{n,m}e^{j\zeta_{n,m}}$  represents channel frequency response from the power transmitter at the  $n^{\text{th}}$  tone and the  $m^{\text{th}}$  antenna. We assume that the information transmitter is an access point transmitting OFDM signals to the information receiver. Following this assumption, the received signal at the nearby information receiver due to the power transmitter is given by

$$y_I(t) = \Re \left\{ \sum_{n=1}^N \mathbf{g}_n \mathbf{w}_n e^{j2\pi f_n t} \right\} + z_I(t) + v_I(t), \quad (4)$$

where  $v_I(t)$  is the noise at the receiver,  $z_I(t)$  is the received OFDM signal due to information exchange given by

$$z_I(t) = \sum_{l=0}^{L-1} a_l \cos(2\pi f_l t + \chi_l), \quad (5)$$

with  $a_l, \chi_l$  being the amplitude and phase of the received OFDM signal, respectively. The number of OFDM sub-carriers is  $L$ , each of frequency  $f_l$  such that  $f_l = f_c + l\Delta f_I$  where  $f_c$  is the carrier frequency and  $\Delta f_I$  is the OFDM sub-carrier spacing.

Communication systems such as Wi-Fi and certain LTE modes use time division duplexing (TDD), which allows the power transmitter to estimate the corresponding CSI for the link to the information receiver (i.e.,  $\mathbf{G}$ ) using the pilots of the information link. The channel to the energy harvester ( $\mathbf{H}$ ) can be estimated in a similar way. For example, the energy harvester can have a beacon phase where it sends a beacon signal (uplink) to the transmitter requesting energy. Assuming reciprocal channels, the power transmitter can use the beacon phase to acquire the CSI to the energy harvester [22]. Backscattering can be an alternative way to estimate the channel to the energy harvester, especially, in wirelessly powered backscatter communication systems [23].

We aim at maximizing the output of the energy harvester and minimizing the interference due to the multi-tone signal at the information receiver. Several energy harvester models exist in the literature; however, for proper modeling in the case of multi-tone excitation, only non-linear energy harvester models should be considered. Different non-linear energy harvester models are discussed and summarized in the following section.

### III. NON-LINEAR ENERGY HARVESTER MODELS

The efficiency of RF energy harvesters is defined as the ratio between between the output DC power of the rectifier and the input RF power to the energy harvester. Due to the presence of non-linear elements (e.g., diodes) in the rectifier as shown in the block diagram of the energy harvester in Fig. 1, the efficiency of the energy harvester is highly dependent on the input power. RF energy harvesters are typically designed to have high conversion efficiency at low input powers (usually few hundreds of  $\mu\text{W}$ ). The input-output power relationship of RF energy harvesters can generally be characterized as shown in Fig. 2. Region 1 in the figure describes the rectifier behavior in the low input power regime. By increasing the input power to the rectifier, the diode elements are driven to the Ohmic linear region (see Region 2) where the diode series resistance is dominant until it saturates and the output power is approximately constant (see Region 3). For linear operation, single-tone excitation can achieve the optimal performance [8], [20]. In addition, no gains can be achieved using multi-tone signals in Region 3 due to the rectifier saturation. Multi-tone excitation becomes important only when the rectifier performance is non-linear, i.e., in Region 1. Different models were proposed in the literature to model the non-linear behavior of the rectifier. They can be divided into two categories: the first category contains models based on the diode non-linearity, and the second contains models based on curve fitting. We will discuss the two different categories in the next two subsections.

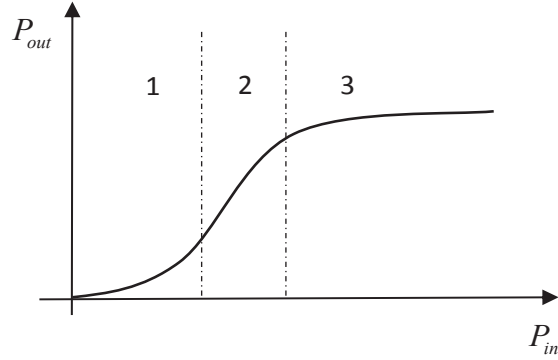


Fig. 2. General input-output relationship of RF energy harvesters.

### A. Rectifier Model Based on Diode Non-Linearity

At the energy harvester, it is assumed that the antenna is perfectly matched to the rectifier circuit. A single-diode rectifier is shown in Fig. 3 where the matching circuit is eliminated due to the assumption of perfect matching. Single-diode rectifiers are used in energy harvesters to minimize the power dissipated in the rectifying components especially at very low input powers. However, voltage doublers are sometimes preferred for full rectification and minimizing the output ripples. Following the assumption of perfect matching, the input voltage to the rectifier circuit can be written from [20], [24] as  $v_{in} = y_p(t) \sqrt{R_{ant}}$ , where  $R_{ant}$  is the antenna impedance. Assuming an ideal diode, the current flowing through the diode is given by

$$i_D = i_s \left( e^{\frac{v_d(t)}{\gamma v_t}} - 1 \right), \quad (6)$$

where  $v_d(t) = v_{in}(t) - v_{out}(t)$ ,  $i_s$  is the saturation current,  $\gamma$  is the non-ideality factor, and  $v_t$  is the diode thermal voltage. Assuming also that the Schottky-based rectifier is in the small-signal operation region (corresponding to Region 1 in Fig. 2) and delivering constant DC output voltage (steady-state response), it follows from the analysis presented in [20], [25], [26] that the output DC current of the rectifier is proportional to the quantity

$$f_{DC} = k_2 R_{ant} \mathbb{E} \{ y_p(t)^2 \} + k_4 R_{ant}^2 \mathbb{E} \{ y_p(t)^4 \}. \quad (7)$$

This expression results from the Taylor expansion of the diode current in (6), with  $k_n$  being the expansion coefficients which can be written as  $k_n = \frac{i_s}{n!(\gamma v_t)^n}$ , and  $n \in \{2, 4\}$ . The Taylor expansion in (7) is terminated to the 4<sup>th</sup> harmonic only which is sufficient to account for the diode non-linearity [17], [18].



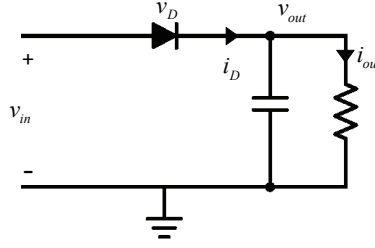


Fig. 3. Single diode rectifier.

### B. Rectifier Model Based on Curve Fitting

As an alternative to modeling the non-linear behavior of the rectifier using the diode non-linear I-V characteristics, one can investigate the non-linearity of the rectifier through the input vs. output power relationship given by  $P_{out} = f(P_{in})$ . Even though the closed form expression for the input-output relation might be unknown, it can be well approximated from simulation data using a data-fitting tool. One of the advantages of using data-fitting models is that they are not limited to a specific energy harvester design; they can be adjusted to fit complicated energy harvester architectures without the need for any assumptions. Three non-linear curve-fitting models are summarized below: the second-order polynomial model [12], the sigmoid model [10], and the rational function model [27], [28].

1) *Second-order polynomial model:* In [12], a model based on data fitting to a second-order polynomial was proposed. Following that model, the input-output power relation can be expressed as:

$$P_{out} = \beta_1 P_{in}^2 + \beta_2 P_{in} + \beta_3, \quad (8)$$

where  $\beta_1$ ,  $\beta_2$  and  $\beta_3 \in \mathbb{R}$  are the parameters of the model which are obtained from curve-fitting tools. The authors in [12] discussed the advantages of the quadratic model for curve fitting by applying it to the energy harvester presented in [16] and showing that this second-order polynomial model is concave with  $\beta_1 \leq 0$ ,  $\beta_2 > 0$ , and  $\beta_3 \leq 0$ . The problem of maximizing the output power of the energy harvester is then formulated as maximizing a concave function (i.e., a convex optimization problem) that can be solved easily with convex optimization tools such as CVX.

The above obtained choice of parameters leads to a convex optimization problem; however, the approximated curve tend to describe the input-output power relationship in Region 2 and Region 3 combined. If this model is to be used in the waveform optimization problem, it should

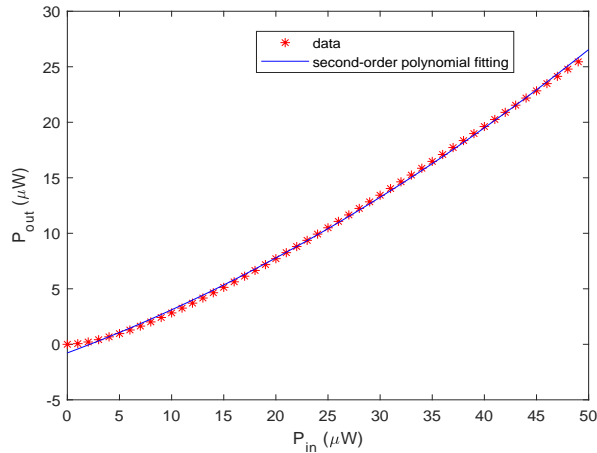


Fig. 4. Second-order polynomial fit based on the simulations of the EH described in Section VI.

be applied to model the behavior of the rectifier in Region 1 as shown in Fig. 4. The data points in the figure are obtained from the simulation results for the rectifier described in Section VI in the low power region. It can be observed from Fig. 4 that the second order polynomial here is convex with  $\beta_1 \geq 0$  and  $\beta_2 > 0$ . Therefore, the problem of maximizing the output power (i.e., maximizing a convex function) in Region 1 leads to a non-convex optimization problem which will be discussed in detail in the next section.

2) *Sigmoid model*: In [10], the non-linear relation between the input power and output power for the energy harvester is modeled by the logistic function given by

$$P_{out} = \frac{\frac{\pi_3}{1+\exp(-\pi_1(P_{in}-\pi_2))} - \frac{\pi_3}{1+\exp(\pi_1\pi_2)}}{1 - \frac{1}{1+\exp(\pi_1\pi_2)}}, \quad (9)$$

where  $\pi_1, \pi_2$ , and  $\pi_3 \in \mathbb{R}$  are the parameters of the model and are obtained through data fitting. This model provides an accurate description for the rectifier behavior in Region 2 and Region 3 which were previously shown in Fig. 2. For proper design of the multi-tone signal, the model should consider the behavior of the rectifier at low input power. Therefore, the sigmoid model does not provide a complete solution to the multi-tone optimization problem. Moreover, the sigmoid model might complicate the multi-tone optimization problem formulation.

3) *Rational function model*: In [28], the authors investigated the possibility to model the non-linear behavior of the rectifier through a rational function defined by

$$P_{out} = \frac{\eta_3 P_{in}^3 + \eta_2 P_{in}^2 + \eta_1 P_{in}}{q_3 P_{in}^3 + q_2 P_{in}^2 + q_1 P_{in} + q_0}, \quad (10)$$

where  $\eta_1, \eta_2, \eta_3, q_0, q_1, q_2$  and  $q_3$  are constants obtained by curve fitting. A modification to this rational function model was introduced by [27] to reduce the number of unknown constants and to simplify the model by writing the input-output relationship as

$$P_{out} = \frac{\theta_3 P_{in} + \theta_2}{P_{in} + \theta_1} - \frac{\theta_2}{\theta_1}, \quad (11)$$

with  $\theta_1, \theta_2$ , and  $\theta_3$  being constants obtained by curve fitting. Similar to the sigmoid model, the rational function models mainly considers the saturation behavior of the rectifier focusing on Region 2 and Region 3, whereas the multi-tone optimization problem becomes interesting in Region 1.

#### IV. WAVEFORM OPTIMIZATION FOR MAXIMUM POWER TRANSFER USING TWO NON-LINEAR RECTIFIER MODELS

In this section, we formulate the optimization problem of designing the multi-tone signal with the goal of maximizing the harvested power from the energy harvester without accounting for the co-existing communication link. For simplicity, we assume at first that the power transmitter is equipped with one antenna ( $M = 1$ ) and then the extension to the case where  $M > 1$  is discussed at the end of this section.

##### A. Single-antenna Case ( $M=1$ )

For  $M = 1$ , we suppress the dependence on  $m$ , and the transmitted power signal becomes

$$x_p(t) = \sum_{n=1}^N s_n \cos(2\pi f_n t + \phi_n) = \Re \left\{ \sum_{n=1}^N s_n e^{j2\pi f_n t} e^{j\phi_n} \right\}, \quad (12)$$

while the received signal at the energy harvester due to the power transmitter becomes

$$y_p(t) = \Re \left\{ \sum_{n=1}^N s_n h_n e^{j2\pi f_n t} e^{j\phi_n} e^{j\psi_n} \right\} = \sum_{n=1}^N s_n h_n \cos(2\pi f_n t + \phi_n + \psi_n). \quad (13)$$

According to [18], [20], [26], the performance of the energy harvester is maximized when all tones have a zero phase when received at the rectifier. Assuming the CSI is known at the power transmitter, the optimum phase for the transmitted waveform will be  $\phi_n^* = -\psi_n$ . Therefore, the received signal at the energy harvester is

$$y_p(t) = \Re \left\{ \sum_{n=1}^N s_n h_n e^{j2\pi f_n t} \right\} = \sum_{n=1}^N s_n h_n \cos(2\pi f_n t). \quad (14)$$

From (14) we can write  $\mathbb{E}\{y_p(t)^2\}$  and  $\mathbb{E}\{y_p(t)^4\}$  which are found in (7) as

$$\mathbb{E}\{y_p(t)^2\} = \frac{1}{2} \sum_{i=1}^N s_i^2 h_i^2, \quad (15)$$

$$\mathbb{E}\{y_p(t)^4\} = \frac{3}{8} \sum_{i=1}^N s_i^4 h_i^4 + \frac{3}{4} \sum_{i=1}^N \sum_{j=1, j \neq i}^N s_i^2 h_i^2 s_j^2 h_j^2. \quad (16)$$

1) *Waveform optimization using diode non-linear model:* Following the non-linear diode model discussed in Section II, the amplitudes of the multi-tone signal can be obtained as solutions to the following optimization problem:

$$\begin{aligned} \max_{\mathbf{s}} \quad & f_{DC}(\mathbf{s}, \phi^*) \\ \text{subject to} \quad & \frac{1}{2} \|\mathbf{s}\|^2 \leq P. \end{aligned} \quad (17)$$

Here  $f_{DC}(\mathbf{s}, \phi^*)$  is obtained from (7) by plugging in (15) and (16). The resulting expression for  $f_{DC}(\mathbf{s}, \phi^*)$  becomes

$$f_{DC}(\mathbf{s}, \phi^*) = k_4 R_{ant}^2 \left( \frac{3}{8} \sum_{i=1}^N s_i^4 h_i^4 + \frac{3}{4} \sum_{i=1}^N \sum_{j=1, j \neq i}^N s_i^2 h_i^2 s_j^2 h_j^2 \right) + k_2 R_{ant} \left( \frac{1}{2} \sum_{i=1}^N s_i^2 h_i^2 \right). \quad (18)$$

Define  $\mathbf{Q} = [Q_{ij}]$  such that  $Q_{ij} = 2(2 - \delta_{ij}) \frac{3k_4 R_{ant}^2}{8} h_i^2 h_j^2$ ,  $\mathbf{a} = \mathbf{1}$  and  $b = 2P$ . We also let  $\mathbf{x} = [s_1^2, s_2^2, \dots, s_N^2]^T$ , and  $\mathbf{f} = \frac{k_2 R_{ant}}{2} [h_1^2, h_2^2, \dots, h_N^2]^T$ . The problem can be re-written in the form of a non-homogeneous linearly constrained quadratic program (LCQP) as follows:

$$\begin{aligned} \max_{\mathbf{x}} \quad & \frac{1}{2} \mathbf{x}^T \mathbf{Q} \mathbf{x} + \mathbf{f}^T \mathbf{x} \\ \text{subject to} \quad & \mathbf{a}^T \mathbf{x} \leq b, \mathbf{x} \geq \mathbf{0}. \end{aligned} \quad (19)$$

Since  $\mathbf{Q}$  is a nonnegative matrix and not necessarily positive semidefinite, the problem is a non-convex LCQP which is known to be  $\mathcal{NP}$  hard [29]. However, for the special case of having a convex quadratic objective function with linear constraints and bounded inputs, this problem can be solved globally using branch and bound methods [29], [30] or integer linear programming [31]. We propose two solutions to the above optimization problem using both methods and show by simulations that the obtained solutions are the same within numerical precision of the simulations; see Section VI.

*Solution using integer linear programming techniques:*

The algorithm proposed in [31] is used as a basis for our proposed solution for (19). In the proposed method, the quadratic program (QP) is reformulated as a linear complementary problem by applying the KKT conditions. Then the complementary constraints are reformulated

using binary variables transforming the optimization problem to a mixed-integer linear problem (MILP) which can be solved effectively using existing MILP solvers such as CPLEX to obtain the QP globally optimal solution.

For the QP in (19), the Lagrange multipliers  $\mu \in \mathbb{R}$  are introduced for the inequality constraint and  $\lambda \in \mathbb{R}^N$  for the non-negativity constraints. The KKT conditions for the problem can be written as

$$\mathbf{Q}\mathbf{x} + \mathbf{f} + \mathbf{a}\mu - \lambda = 0 \quad (20)$$

$$\mathbf{x}^T \lambda = 0 \quad (21)$$

$$\mu (\mathbf{a}^T \mathbf{x} - b) = 0 \quad (22)$$

$$\mathbf{x} \geq \mathbf{0}, \lambda \geq \mathbf{0}, \mu \geq 0. \quad (23)$$

Since the problem is non-convex, these are only first order necessary conditions for the optimal solution of (19). The KKT conditions can be added as constraints the original problem in (19) to obtain the following equivalent<sup>1</sup> formulation:

$$\max_{\mathbf{x}, \lambda, \mu} \frac{1}{2} \mathbf{x}^T \mathbf{Q}\mathbf{x} + \mathbf{f}^T \mathbf{x}$$

$$\text{subject to } \mathbf{Q}\mathbf{x} + \mathbf{f} + \mathbf{a}\mu - \lambda = 0 \quad (24)$$

$$\mathbf{x}^T \lambda = 0, \mu (\mathbf{a}^T \mathbf{x} - b) = 0$$

$$\mathbf{x} \geq \mathbf{0}, \lambda \geq \mathbf{0}, \mu \geq 0.$$

As shown in [29], [31], the KKT conditions (20)-(22) can be used to linearize the objective of (24) as follows,

$$\begin{aligned} \frac{1}{2} \mathbf{x}^T \mathbf{Q}\mathbf{x} + \mathbf{f}^T \mathbf{x} &= \frac{1}{2} (\mathbf{f}^T \mathbf{x} - \mathbf{x}^T \mathbf{a}\mu + \mathbf{x}^T \lambda) \\ &= \frac{1}{2} (\mathbf{f}^T \mathbf{x} - b\mu). \end{aligned} \quad (25)$$

The optimization problem becomes,

$$\max_{\mathbf{x}, \lambda, \mu} \frac{1}{2} (\mathbf{f}^T \mathbf{x} - b\mu)$$

$$\text{subject to } \mathbf{Q}\mathbf{x} + \mathbf{f} + \mathbf{a}\mu - \lambda = 0 \quad (26)$$

$$\mathbf{x}^T \lambda = 0, \mu (\mathbf{a}^T \mathbf{x} - b) = 0$$

$$\mathbf{x} \geq \mathbf{0}, \lambda \geq \mathbf{0}, \mu \geq 0.$$

<sup>1</sup>Two optimization problems are equivalent if the solution to one can be obtained from the other, and vice-versa.

The difficulty of solving this problem is due to the coupling among the variables of  $\mathbf{x}^T \boldsymbol{\lambda} = 0$ . A solution method to this problem was proposed in [31] by solving the following equivalent MILP:

$$\begin{aligned} & \max_{\mathbf{x}, \boldsymbol{\lambda}, \mu} \frac{1}{2} (\mathbf{f}^T \mathbf{x} - b\mu) \\ & \text{subject to } \mathbf{Q}\mathbf{x} + \mathbf{f} + \mathbf{a}\mu - \boldsymbol{\lambda} = 0 \\ & 0 \leq \mathbf{x} \leq z\mathbf{u}, 0 \leq \boldsymbol{\lambda} \leq (1-z)\mathbf{v}, \\ & \mu (\mathbf{a}^T \mathbf{x} - b) = 0, z \in \{0, 1\}, \end{aligned} \quad (27)$$

where  $\mathbf{u}, \mathbf{v} \in \mathbb{R}^N$  are the upper bounds on the the decision variables  $\mathbf{x}, \boldsymbol{\lambda}$  such that there are globally optimal KKT points  $(\mathbf{x}, \mu, \boldsymbol{\lambda})$  for the primal QP satisfying  $\mathbf{x} \leq \mathbf{u}, \boldsymbol{\lambda} \leq \mathbf{v}$ . The upper bound  $\mathbf{u}$  is given by  $\mathbf{u} = \mathbf{x}^*$ , where  $\mathbf{x}^*$  is the solution to the following linear programming (LP) problem:

$$\begin{aligned} & \max_{\mathbf{x}} \quad \mathbf{x} \\ & \text{subject to } \quad \mathbf{a}^T \mathbf{x} \leq b, \mathbf{x} \geq \mathbf{0}, \end{aligned} \quad (28)$$

and  $\mathbf{v} = \boldsymbol{\lambda}^*$ , with  $\boldsymbol{\lambda}^*$  being the solution to the LP problem given by

$$\begin{aligned} & \max_{\boldsymbol{\lambda}} \quad \boldsymbol{\lambda} \\ & \text{subject to } \quad \mathbf{Q}\mathbf{x} + \mathbf{f} + \mathbf{a}\mu - \boldsymbol{\lambda} + \boldsymbol{\rho} = 0 \\ & \quad \quad \quad 0 \leq \mathbf{X} \leq \mathbf{u}\mathbf{u}^T \\ & \quad \quad \quad 0 \leq \mathbf{x} \leq \mathbf{u}, \boldsymbol{\lambda}, \boldsymbol{\rho} \geq 0, \mathbf{X} \in S^N, \end{aligned} \quad (29)$$

where  $S^N$  represents the set of  $N \times N$  real symmetric matrices. The matrix  $\mathbf{X}$  represents the linearization of the matrix  $\mathbf{x}\mathbf{x}^T \in S^N$ , and  $\boldsymbol{\rho} \in \mathbb{R}^N$  is a dual variable introduced to calculate the bound. Solving the LP in (28) and (29), the obtained bounds are then applied to the MILP in (27), and then solving this equivalent problem using MILP solvers such as CPLEX [31] yields to obtaining an optimal solution to the primal problem given by (19).

*Solution using branch-and-bound-technique:*

A globally optimal solution to non-convex quadratic programs using a finite branch-and-bound method was presented in [29], [30]. Optimality is achieved by enforcing the first-order KKT conditions through branching and then solving a convex relaxation of the quadratic program at each node of the branch-and-bound tree. Two types of relaxations were discussed by Burer and Vanderbussche [29], namely Linear program (LP) relaxation and a semidefinite program (SDP) relaxation. We will start by describing the solution using the LP relaxation approach and then describe the SDP formulation.

The feasible set of (19) is referred to as

$$\mathcal{P} := \{\mathbf{x} \in \mathbb{R}^N : \mathbf{a}^T \mathbf{x} \leq b, \mathbf{x} \geq \mathbf{0}\}. \quad (30)$$

The solution starts by introducing the the Lagrange multipliers  $\mu \in \mathbb{R}$  for the inequality constraint and  $\boldsymbol{\lambda} \in \mathbb{R}^N$  for the non-negativity constraints of the QP in (19) and then writing the first-order KKT conditions in the same way as (20)-(23). Then, two sets  $\mathcal{G}$  and  $\mathcal{C}$  are defined as:

$$\mathcal{G} := \{(\mu, \boldsymbol{\lambda}) \geq 0 : \boldsymbol{\lambda} - \mathbf{a}\mu = \mathbf{Q}\mathbf{x} + \mathbf{f}\}, \quad (31)$$

$$\mathcal{C} := \{(\mu, \boldsymbol{\lambda}) \geq 0 : \mu(\mathbf{a}^T \mathbf{x} - b) = 0, \mathbf{x}^T \boldsymbol{\lambda} = 0\}. \quad (32)$$

Any local optimal solution  $\mathbf{x}$  must satisfy  $\mathcal{G} \cap \mathcal{C} \neq \emptyset$ . Following (25), the optimization problem can be reformulated in a similar way to (26) as

$$\begin{aligned} & \max_{\mathbf{x}} \frac{1}{2} (\mathbf{f}^T \mathbf{x} - b\mu) \\ & \text{subject to } \mathbf{x} \in \mathcal{P}, (\mu, \boldsymbol{\lambda}) \in \mathcal{G} \cap \mathcal{C}. \end{aligned} \quad (33)$$

The formulation in (33) allows the use of finite branch-and-bound, where the complementary constraints are enforced using linear equations. At each node of the tree, two index sets are introduced  $\mathcal{F}^x, \mathcal{F}^\lambda \subseteq \{1, \dots, n\}$  which satisfy  $\mathcal{F}^x \cap \mathcal{F}^\lambda = \emptyset$ . These two index sets are used to enforce the complementary constraints by solving the following LP optimization problem:

$$\begin{aligned} & \max_{\mathbf{x}} \frac{1}{2} (\mathbf{f}^T \mathbf{x} - b\mu) \\ & \text{subject to } \mathbf{x} \in \mathcal{P}, (\mu, \boldsymbol{\lambda}) \in \mathcal{G} \cap \mathcal{C} \\ & \quad x_i = 0, i \in \mathcal{F}^x \\ & \quad \lambda_i = 0, i \in \mathcal{F}^\lambda \\ & \quad \mathbf{a}^T \mathbf{x} - b = 0, \mu = 0. \end{aligned} \quad (34)$$

The constraint  $(\mu, \boldsymbol{\lambda}) \in \mathcal{C}$  can be dropped to obtain an LP relaxation. This relaxation maintains complementary because  $x_i \lambda_i = 0$  for all  $i \in \mathcal{F}^x \cup \mathcal{F}^\lambda$ . Branching on a node is done by selecting some  $i \in \{1, \dots, n\} \setminus \mathcal{F}^x \cup \mathcal{F}^\lambda$  and then creating two children by adding  $i$  to  $\mathcal{F}^x$  for one child and  $i$  to  $\mathcal{F}^\lambda$  for the other [29], [32]. Adding indices progressively enforces more complementarity at nodes deeper in the tree. It should be noted that the root node in the branch tree has all index sets empty.

SDP relaxations are known to be bounded. That is why they are preferred to LP relaxations in finite branch-and-bound algorithms. Instead of solving a LP at each node, the QP in (19) is reformulated in the form of a relaxed SDP as follows,

$$\max_{\mathbf{X}, \mathbf{x}} \frac{1}{2} \text{tr}(\mathbf{Q}\mathbf{X}) + \mathbf{f}^T \mathbf{x} \quad (35)$$

$$\text{subject to } \mathbf{a}^T \mathbf{x} \leq b, \mathbf{X} \succeq \mathbf{x}\mathbf{x}^T, \mathbf{X} \geq \mathbf{0}, \mathbf{x} \geq \mathbf{0},$$

where  $\mathbf{X} \geq \mathbf{0}$  denotes a positive semidefinite matrix. The complementary constraints are then added to the above SDP as in (34) and enforced through branching. Finite branch-and-bound using SDP was proven to globally solve non-convex QCQP [29]. However, it has high computational complexity due to solving a SDP at each node of the BB tree. On the other hand, in the MILP technique, the dual bounds are calculated and the equivalent problem is solved using CPLEX once. Since the work proposed in [31] is still under review, we implemented both solution methods to show that the MILP technique can be used to obtain a globally optimal solution for our multi-tone optimization problem.

**Computational Complexity:** Evidently, obtaining globally optimal solutions for a non-convex problem comes at the cost of elevated complexity for the algorithms. Here, we make approximate complexity calculations for both the BB and MILP solutions. The computational complexity of the BB methods is dominated by solving the SDP, in (35): this can be done using generic solvers with  $\approx \mathcal{O}(N^4)$ , for each node in the BB tree. Assuming a total maximum of BB nodes of  $K$ , the total complexity of the BB algorithm is  $\approx K\mathcal{O}(N^4)$  operations. On the other hand, obtaining similar complexity calculations is more challenging for our MILP solution, since the complexity of MILP is harder to characterize in closed-form expressions. We note that complexity reduction techniques are interesting future work, namely, interior point method to reduce the complexity of (35), and heuristics to obtain locally optimal solutions to the non-convex QP.

2) *Waveform optimization using curve-fitting model:* The second-order polynomial model given by (8) can be slightly modified in the case of multi-tone excitation in the following way:

$$P_{out}(t) = \beta_1 P_{in}^2(t) + \beta_2 P_{in}(t) + \beta_3, \quad (36)$$

where  $P_{in}(t) = y_p^2(t)$  is the instantaneous input power to the energy harvester. It is required to maximize the average output power of the energy harvester given by  $P_{out} = \mathbb{E}\{P_{out}(t)\}$ . By averaging Eq. (36) the output DC power of the rectifier can be written as:

$$P_{out} = \beta_1 \mathbb{E}\{y_p(t)^4\} + \beta_2 \mathbb{E}\{y_p(t)^2\} + \beta_3, \quad (37)$$



with  $\mathbb{E}\{y_p(t)^2\}$ ,  $\mathbb{E}\{y_p(t)^4\}$  expressed in the same way as (15) and (16), respectively. Following the assumption of perfect CSI at the power transmitter and substituting by the optimal phases given by  $\phi_n^* = -\psi_n$ , the multi-tone optimization problem in the case of the modified second order polynomial model based becomes:

$$\begin{aligned} & \max_{\mathbf{s}} \beta_1 \left( \frac{3}{8} \sum_{i=1}^N s_i^4 h_i^4 + \frac{3}{4} \sum_{i=1}^N \sum_{j=1, j \neq i}^N s_i^2 h_i^2 s_j^2 h_j^2 \right) + \beta_2 \left( \frac{1}{2} \sum_{i=1}^N s_i^2 h_i^2 \right) \\ & \text{subject to } \frac{1}{2} \|\mathbf{s}\|^2 \leq P. \end{aligned}$$

Again, defining  $\mathbf{x} = [s_1^2, s_2^2, \dots, s_N^2]^T$ , the problem can be written in the form of a non-convex LCQP in a similar way to (19) and solved as described before.

### B. Extension to MISO Power Transfer ( $M > 1$ )

When  $M > 1$ , the expressions given in (15) and (16) do not hold and the problem in this case cannot be formulated as a LCQP. However, a simple trick can be applied to decouple the frequency and the space domains without affecting the performance [20]. Noticing that the optimal phases for maximizing the output of the energy harvester are given by  $\phi_{n,m}^* = -\psi_{n,m}$ , one can generalize this to express the optimal weight vector represented by  $\mathbf{w}_n$  as the matched beamformer given by

$$\mathbf{w}_n = s_n \frac{\mathbf{h}_n^H}{\|\mathbf{h}_n\|}. \quad (38)$$

Applying the weight vector from (38) to (3), the MISO channel is converted to the equivalent scalar channel and the received signal at the energy harvester becomes

$$y_p(t) = \Re \left\{ \sum_{n=1}^N s_n \|\mathbf{h}_n\| e^{j\omega_n t} \right\}. \quad (39)$$

The transmitter power constraint remains the same as  $\frac{1}{2} \|\mathbf{s}\|^2 \leq P$ . This allows the formulation of the optimization problem as a LCQP by replacing each  $h_n$  in (15) and (16) by  $\|\mathbf{h}_n\|$  which can be interpreted as the effective channel gain at frequency  $n$ . The optimal amplitude of the  $n^{\text{th}}$  tone given by  $s_n$  is then obtained by solving the LCQP as described previous subsections either by applying the diode model or the curve-fitting model.

## V. WAVEFORM OPTIMIZATION FOR IN-BAND SWIPT

### A. Problem Motivation

In this section, we consider the co-existing communication link described in Fig. 1. One of the important building blocks in the RF front end of any information receiver is the LNA which amplifies the received RF signal before the mixing and filtering stages to extract the baseband signal. LNAs are active components having a non-linear behavior. However, they are designed to operate linearly within a certain power range corresponding to the received communication signals. At power levels higher than the specific design range, the LNA of the information receiver saturates and exhibits a non-linear behavior producing inter-modulation products and high-order harmonics. For example, if two signals are received at frequencies  $f_1$  and  $f_2$ , the inter-modulation products appear at frequencies  $f_{i,j} = \pm i f_1 \pm j f_2$  where  $i, j$  are positive integers. The order of the inter-modulation product is defined by  $i + j$ . Usually, the third order inter-modulation products given by  $2f_1 - f_2$  and  $2f_2 - f_1$  are the most problematic [33]. This is because if  $f_1$  and  $f_2$  are close to each other, the third order inter-modulation products may fall inside the channel of interest with a high power level that is enough to block it as shown in Fig. 5. As power signals are usually transmitted at a higher power level than communication signals, the sub-carrier frequencies in the multi-tone signal are chosen such that they do not interfere with any information sub-carrier or interfere at most with one sub-carrier as discussed in [34]. However, from the experiment described in the introduction, this was found to be not enough to preserve the communication link and the data rates. In case of in-band SWIPT, the inter-modulation products of the multi-tone signal are more likely to fall inside the channel of interest causing interference. Therefore, it is necessary to prevent the LNA of the information receiver from saturation and keep it in its linear operation region.

In RF applications, the input impedance of active components changes significantly with the input power, which makes the matching effect more critical. For this reason, it is more common to express the constraints on the non-linearity of RF amplifiers in terms of power constraints instead of voltage constraints, namely the 1-dB compression point ( $P_{1\text{dB}}$ ) and the third-order intercept ( $IP_3$ ) point. According to [33],  $P_{1\text{dB}}$  is defined as the input power at which the amplifier gain drops by 1 dB from the normal linear gain. It provides a value for the input power at which the amplifier goes into compression and becomes saturated. The  $IP_3$  point indicates the value of the input power at which the amplitude of the third-order inter-modulation products becomes

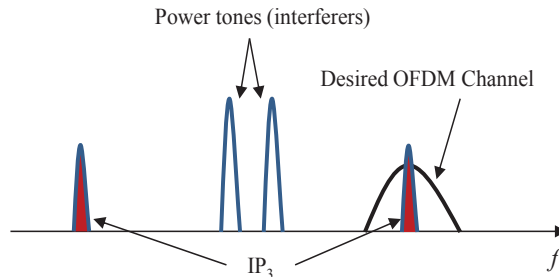


Fig. 5. Distortion and blocking due to third-order inter-modulation products.

equal to the input signal. For a LNA to maintain its linear behavior, the input power should be below the 1-dB compression point (a typical value for  $P_{1\text{dB}}$  at 2.4 GHz is around -15 dBm) and sufficiently lower than the  $IP_3$  point.

### B. Formulating the Optimization Problem

1) *Single antenna case* : Based on the above discussion, we add a constraint on the received power at the nearby communication receiver  $P_{sat}$  to prevent its LNA from saturation. Considering the case where  $M = 1$ , the received signal at the information receiver due to the power transmitter from (4) becomes

$$y_{IP}(t) = \Re \left\{ \sum_{n=1}^N s_n g_n e^{j2\pi f_n t} e^{j\phi_n} e^{j\zeta_n} \right\}. \quad (40)$$

Therefore, the average power received is given by  $\mathbb{E} \{y_{IP}(t)^2\}$  and can be written as  $\frac{1}{2} \sum_{n=1}^N s_n^2 g_n^2$ . Adding the received power constraint<sup>2</sup> to the optimization problem results in,

$$\begin{aligned} & \max_{\mathbf{s}} \quad f_{DC}(\mathbf{s}, \phi^*) \\ & \text{subject to} \quad \frac{1}{2} \|\mathbf{s}\|^2 \leq P, \quad \frac{1}{2} \sum_{n=1}^N s_n^2 g_n^2 \leq P_{sat}. \end{aligned} \quad (41)$$

After reformulating the problem in the form of LCQP we re-write the optimization problem as

$$\begin{aligned} & \max_{\mathbf{x}} \quad \frac{1}{2} \mathbf{x} \mathbf{Q} \mathbf{x}^T + \mathbf{f}^T \mathbf{x} \\ & \text{subject to} \quad \begin{bmatrix} \mathbf{1}^T \\ \mathbf{v} \end{bmatrix} \mathbf{x} \leq \begin{bmatrix} 2P \\ 2P_{sat} \end{bmatrix} \\ & \quad \mathbf{x} \geq \mathbf{0}, \end{aligned} \quad (42)$$

<sup>2</sup>It should be noted that the received power due to the legitimate information link also contributes towards the LNA saturation. Therefore, the constraint  $P_{sat}$  should actually be lower than  $P_{1\text{dB}}$ , i.e.,  $P_{sat} = P_{1\text{dB}} - \varepsilon$ , where  $\varepsilon$  represents the average power received due to the information signal.

where  $\mathbf{v} = [g_1^2, g_2^2, \dots, g_n^2]$ . By defining  $\mathbf{A}_2 = \begin{bmatrix} \mathbf{1}^T \\ \mathbf{v} \end{bmatrix}$  and  $\mathbf{b}_2 = [2P \quad 2P_{sat}]^T$ , the problem can be solved in the same procedure described in Section III.

2) *MISO case* ( $M > 1$ ): Although the matched beamformer given by (38) maximizes the received power at the energy harvester, it does not take into account co-existing information transmitters and receivers. The received signal at the nearby information receiver after applying this matched beamformer becomes

$$y_{IP}(t) = \Re \left\{ \sum_{n=1}^N s_n \mathbf{g}_n \frac{\mathbf{h}_n^H}{\|\mathbf{h}_n\|} e^{j2\pi f_n t} \right\}. \quad (43)$$

As the number of transmitting antennas  $M$  increases, the radiated beam for power transmission becomes narrower and more directed towards the energy harvester, thus, limiting the amount of power received at the information receiver. This can also be viewed from the value of  $\mathbb{E} \{ \mathbf{g}_n \mathbf{h}_n^H \mathbf{h}_n \mathbf{g}_n^H \}$  which tends to zero as  $M$  increases (by the law of large numbers). Nevertheless, the possible interference resulting from the matched beamformer is still captured in the constraint given by  $\mathbb{E} \{ y_{IP}(t)^2 \} \leq P_{sat}$ . One may also think of a hybrid beamforming scheme in which the weighting vector is a linear combination of the matched beamformer and the zero-forcing beamformer as in MISO interference channels [35], [36]. However, by expressing the weighting vector as a linear combination of these two beamformers, the multi-tone optimization problem becomes intractable and cannot be formulated as a LCQP. The problem of global optimal multi-tone multi-antenna SWIPT remains interesting for future research.

## VI. SIMULATION RESULTS

Consider a WPT system with  $N = 8$  tones. We start by assuming a SISO system with  $M = 1$  and comparing our MILP and BB solutions to the multi-tone optimization problem to three strategies for power allocation to different tones. The first strategy is the equal amplitude splitting (Equal AS), i.e., to divide power equally among all tones such that  $s_n = \sqrt{\frac{2P}{N}}$ . The second strategy is the maximum-ratio transmission (MRT) in which the amplitude of the  $n^{th}$  tone is given by  $s_n = h_n \sqrt{\frac{2P}{\sum_{i=1}^N h_i^2}}$ . The third is the adaptive single sinewave, in which all the power is allocated to the tone corresponding to the strongest channel  $h_{n^*}$  with  $n^* = \arg \max_n h_n$ , i.e.,  $s_{n^*} = \sqrt{2P}$ . We also compare our solution to the one proposed in [20] using reverse geometric programming (Reverse GP). Details of reverse geometric programming solution method are omitted from this paper, since it was implemented only for comparison reasons. We consider a

Rician channel model motivated by the fact that for efficient WPT systems LOS should exist between the wireless power transmitter and the energy harvester. We modified the channel model in [8] to be  $h_n = \sqrt{L_P}Z$ , where  $Z \sim \mathcal{CN}\left(\sqrt{\frac{\kappa}{\kappa+1}}, \frac{1}{\kappa+1}\right)$ . Here,  $L_P$  represents the path loss given by  $\left(\frac{\lambda}{4\pi d}\right)^2$  with  $d$  being the distance between the transmitter and the receiver,  $\lambda$  is the wavelength at the carrier frequency, and  $\kappa$  is the Rice factor. We assume that  $\kappa_{(dB)} = 3$  dB and that the channel frequency responses  $h_n$  are independent. The antenna gains are eliminated from the considered channel model and assumed to be unity. We assume that  $f_o = 2.4$  GHz,  $\Delta f_p = 1.25$  MHz and the energy harvester is at distance  $d = 8\lambda$  from the transmitter. We assume that  $R_{ant} = 50 \Omega$ . We first present the results for maximizing the output of the energy harvester using the diode non-linear model and the curve-fitting model. Then, we consider the co-existing communication link.

The power levels chosen for simulations in this paper are within the the Federal Communications Commission (FCC) safety regulations. For example, FCC allows a maximum of 4 W equivalent isotropic radiated power (EIRP) on the 2.4 GHz band. This permits the reception of power that can reach higher than  $100 \mu\text{W}$  at an energy harvester placed at distance  $8\lambda$ . The regulations vary in different countries. In Sweden, for example, the maximum EIRP allowed at 2.4 GHz is 100 mW. However, a maximum EIRP of 500 mW is allowed for powering RFID tags in the band 2.446 GHz to 2.454 GHz. These regulations have been taken care of when conducting experiments such as the one mentioned in the introduction to this paper. It is worth mentioning that all the current standardization is defined for communication networks but no standardization has been defined for wireless power transfer so far.

#### A. Results for Maximizing the Output of the Energy Harvester

1) *Diode model:* The diode characteristics are obtained from the SMS-7630 data sheet. This diode, provided by Skyworks, is known to have a low turn-on voltage (i.e., it can be as low as 60 mV) which minimizes the power consumption, and hence, improves the RF-to-DC conversion efficiency at low-input power levels. Following this, we assume  $i_s = 5 \mu\text{A}$ ,  $v_t = 25.86$  mV, and  $\gamma = 1.05$ . For implementing the reverse geometric programming method, the relative error threshold was selected to be  $\epsilon = 10^{-6}$ .

In Fig. 6a, the frequency response (normalized to  $h_{max}$ ) of one possible realization of the assumed channel is plotted. We normalize the transmitted power  $P$  to the path loss  $L_P$  to represent the maximum possible received power at the energy harvester and denote it by  $P_{EH}$ .

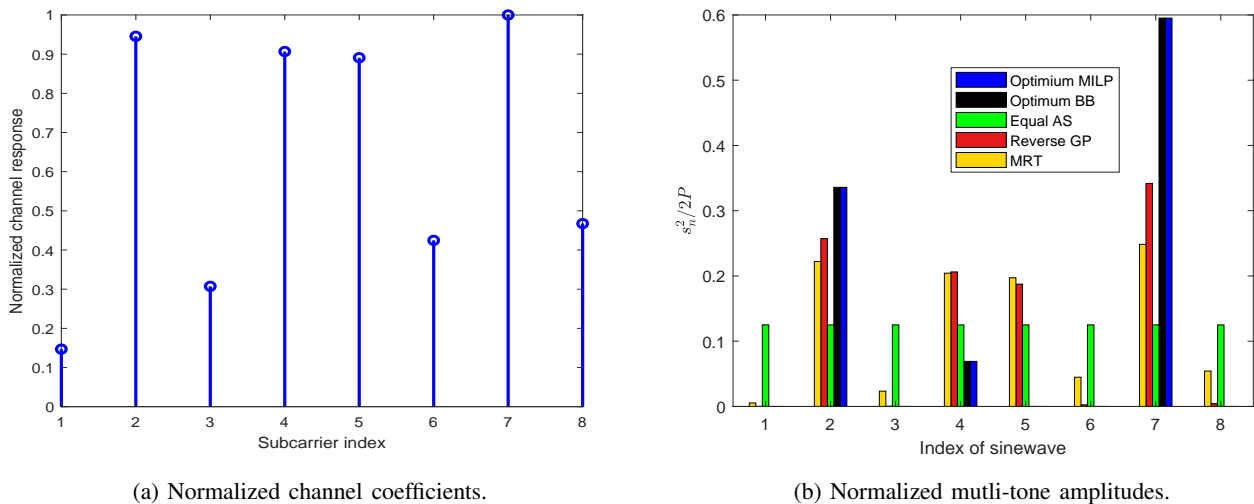


Fig. 6. Power allocation to different tones resulting from the diode model for one possible channel realization at  $P_{EH} = 50 \mu\text{W}$ .

For this particular realization shown in Fig. 6a and for  $P_{EH} = 50 \mu\text{W}$ , the power allocated to each tone resulting from the different power allocation strategies is shown in Fig. 6b normalized to the total power given by  $P$ . It can be observed that the optimal strategy tends to allocate power to tones having the strongest channels. Both optimal schemes show the same results; power is divided proportionally among the three strongest tones. It should also be mentioned that as the transmitted power increases, the optimal schemes starts allocating power to the next strong tone. Reverse GP tends to show a behavior similar to MRT as can be observed from the results in Fig. 6b and from the discussion in [20], [37]. Since the output current is proportional to  $f_{DC}$ , we refer to  $f_{DC}$  as the output current in the rest of this section. In Fig. 7, the average output current (over many channel realizations) is plotted vs. the transmitted power for different power allocation strategies. It can be noticed that our solution to the optimization problem achieves the maximum possible output current for a given input power among all other power allocation strategies. For example, at  $P_{EH} = 50 \mu\text{W}$ , using the optimal schemes can improve the output current from the energy harvester by approximately  $0.5 \mu\text{A}$  ( $\approx 4\%$  increase) compared to the Reverse GP solution. As the transmitted power increases (accordingly  $P_{EH}$  increases), higher gains can be obtained by applying the optimal allocation strategies. It can also be observed from both Fig. 6b and Fig. 7 that the solutions obtained from MILP and finite BB methods coincide with each other.

In Fig. 8, we evaluate the performance of different allocation strategies with an approximately frequency-flat channel generated by letting  $h_n \sim \mathcal{N}(1, 0.05)$ . By varying the transmitted power

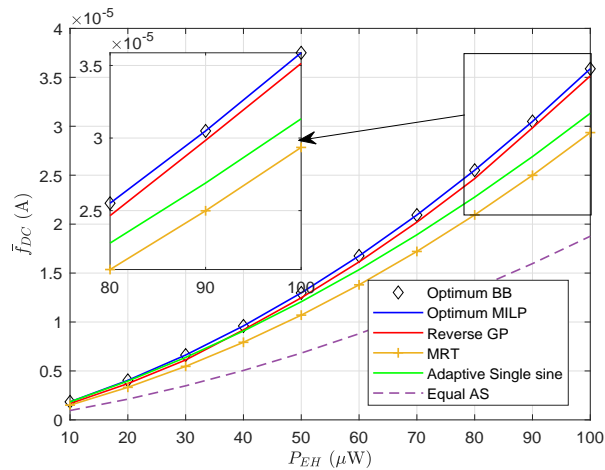


Fig. 7. Average output current (over many channel realizations) represented by  $\bar{f}_{DC}$  vs. transmitted power (normalized to path loss) for  $M = 1$ .

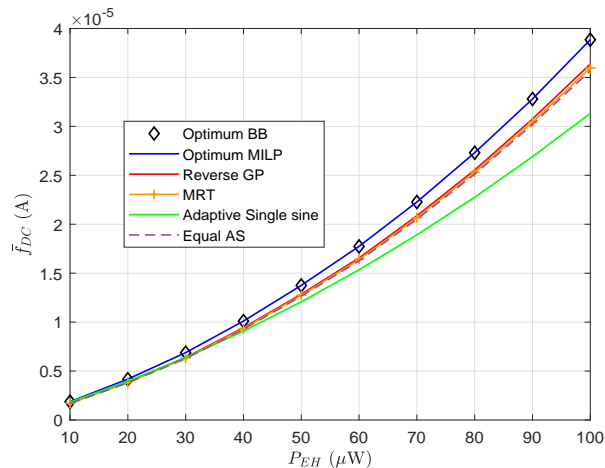


Fig. 8. Average output current represented by  $\bar{f}_{DC}$  vs. normalized transmitted power in the case of an approximately frequency-flat Channel.

and observing the output DC current, it can be noticed that MRT and Equal AS strategies have better performance than adaptive single sine strategy, opposite to the frequency-selective channel case. It can also be observed that the gains obtained by applying the optimal strategies in this case are higher compared to Fig. 7. The output current can be improved by approximately  $1 \mu\text{A}$  ( $\approx 7\%$  increase) at  $P_{EH} = 50 \mu\text{W}$  compared to the Reverse GP solution. In the case of a perfectly flat channel (i.e., all channel coefficients are exactly the same), the optimal strategy, of course, is to split power equally among all tones which is obtained from MRT, Equal AS, optimum MILP, optimum BB, and Reverse GP strategies.

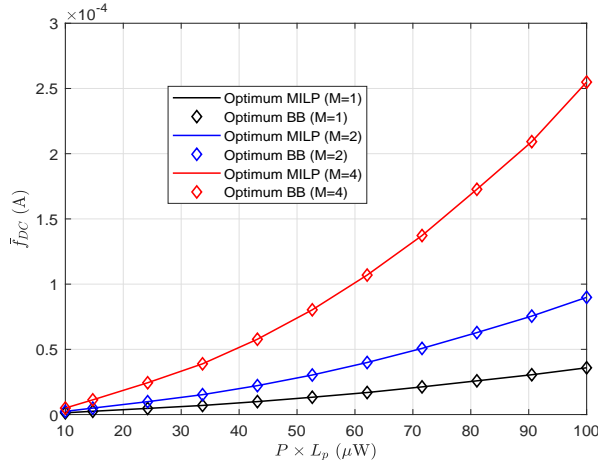


Fig. 9. Comparison of the average output current (over many channel realizations) represented by  $\bar{f}_{DC}$  vs. transmitted power (normalized to path loss) for different values of  $M$ .

The effect of increasing the number of antennas at the transmitter on the output of the energy harvester is investigated in Fig. 9<sup>3</sup>. The output current of the energy harvester is plotted vs.  $P \times L_p$  which is the same as  $P_{EH}$  described for  $M = 1$ . However, it is more accurate to express it in this way in the MISO case since the maximum possible received power at the energy harvester differs from the SISO case due to the array gain (beamforming gain). As expected, increasing the number of transmitting antennas, increases the output current of the energy harvester.

2) *Curve-fitting model based on circuit simulations*: In order to evaluate the performance of the second-order polynomial curve-fitting model discussed in Section IV. A single-diode rectifier circuit was designed and simulated to achieve its maximum efficiency at  $50 \mu\text{W}$  using Keysight Technologies Advanced Design Systems (ADS). The designed rectifier is shown in Fig. 10. The choice of the output capacitor and resistor affects the low-pass filtering characteristics of the rectifier. In order to deliver a smooth DC output, the RC circuit time constant  $\tau = R_L C_{out}$  should be chosen to be sufficiently larger than  $\frac{1}{\Delta f_P}$ . The values of  $C_1$  and  $L_1$  are calculated according to L-matching circuit formulas [33] in order to match the rectifier to the  $50 \Omega$  antenna. As mentioned before in Section III, due to the presence of the non-linear diode, the input impedance of the rectifier circuit varies with varying the input power to the rectifier. It is difficult to keep a good level of matching for a wide range of input powers with a simple design, especially at very low-

<sup>3</sup>Due to the high complexity in implementing the reverse geometric programming for  $M > 1$  and the unavailability of the code for reuse, we only show results for MISO WPT using our optimal schemes.



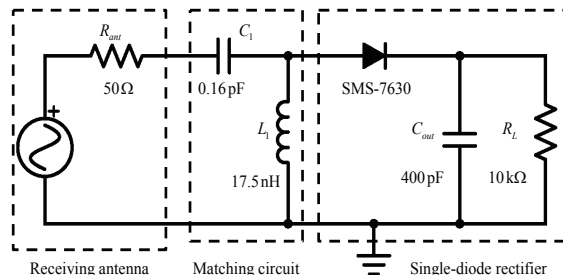


Fig. 10. Single-diode rectifier with L-matching network.

input power. That is why, the rectenna is optimized to have its maximum efficiency at a certain input power level. Large Signal S-Parameters (LSSP) and Harmonic Balance (HB) simulators in ADS were used to calculate the input impedance for matching and calculate the output DC power, respectively.

Second-order polynomial fitting using MATLAB was applied to the simulated input-output power characteristics as previously shown in Fig. 4 to calculate the values of  $\beta_1$  and  $\beta_2$  in (8). Using the same channel realization in Fig. 6a, for  $M = 1$  and  $P_{EH} = 50 \mu\text{W}$ , the power allocated to each tone (normalized to the total transmitted power) obtained from solving the optimization problem resulting from the curve-fitting model is shown in Fig. 11a. It can be observed that power is allocated to different tones in a similar way as in the case of the diode model. The small difference comes from the fact that  $\beta_1 \neq k_4 R_{ant}^2$  and  $\beta_2 \neq k_2 R_{ant}$ . The simulated average output DC power is plotted vs. the normalized transmitted power in Fig. 11b emphasizes the improvement achieved by optimizing multi-tone excitation. The results shown in Fig. 11a and Fig. 11b prove that the second-order curve-fitting model can be used as an alternative model for the multi-tone optimization problem.

### B. Results for In-Band SWIPT

Finally, we consider the co-existing communication link by taking into account the saturation power of the LNA of the nearby information receiver. A single antenna is assumed at the power transmitter. The diode model is adopted for simulations in this subsection. The normalized transmitted power (maximum possible received power at the energy harvester) is fixed to  $P_{EH} = 100 \mu\text{W}$ . We first assume that the saturation power  $P_{sat} = -15 \text{ dBm}$ , and that the nearest information receiver is located at  $d_2 = 7\lambda$ , i.e., closer to the power transmitter from the energy harvester. Accordingly, a possible realization of the channel coefficients  $h$  and  $g$  normalized to

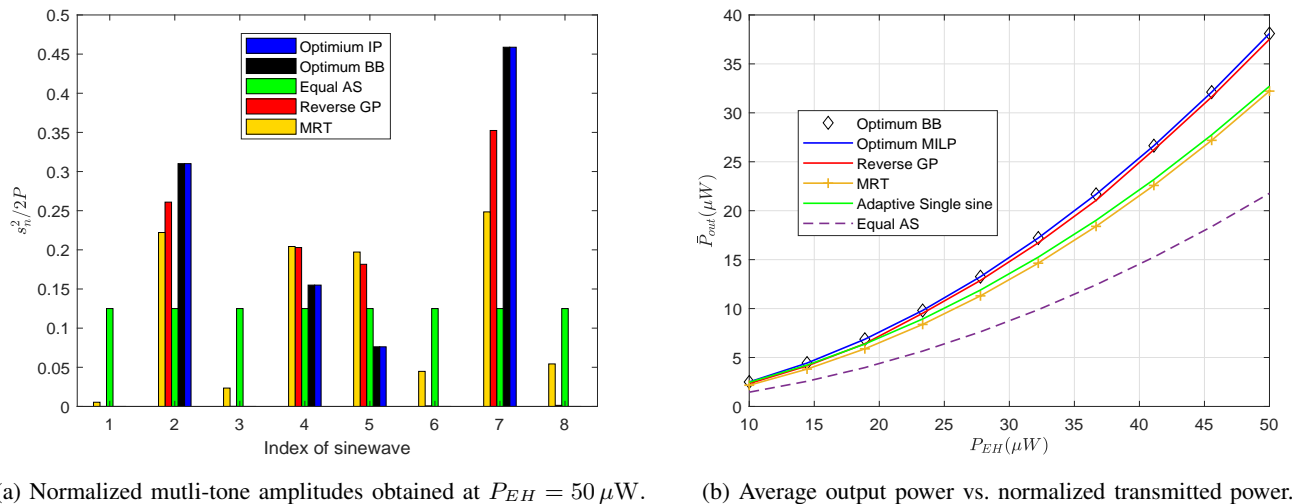
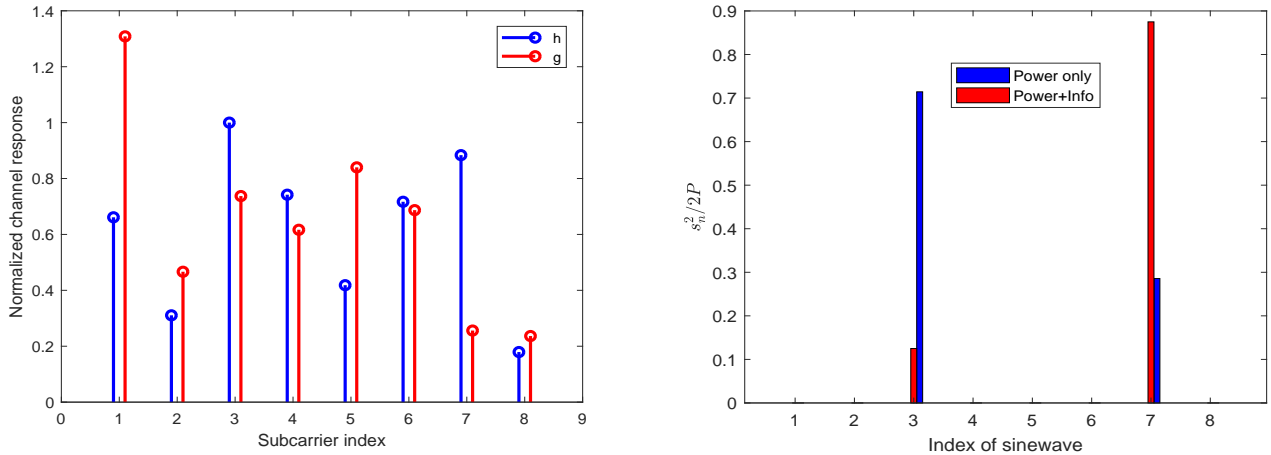


Fig. 11. Simulation results for the second-order polynomial curve-fitting model.

$h_{max}$  is plotted in Fig. 12a. The corresponding optimal power allocation strategy with and without considering the information link is shown in Fig. 12b. It can be observed from the figure that although sub-carrier#3 has a stronger channel to the energy harvester than subcarrier#7, the latter has been allocated more power when considering the co-existing communication link because it has a weaker channel to the information receiver. By varying the transmitted power, the average output current is plotted in Fig. 13. Taking the saturation power into consideration affects the maximum possible output current when increasing the transmitted power. The saturation power is varied in Fig. 14a and the average output current is observed. Of course, as the saturation power increases, the achievable output current increases until it coincides with the case when having the energy harvester only. In Fig. 14b, the effect of the distance of the information receiver from the power transmitter is studied. It can be observed that the effect of the  $P_{sat}$  on the maximum achievable output current decreases as the distance of the nearest information receiver from the power transmitter increases.

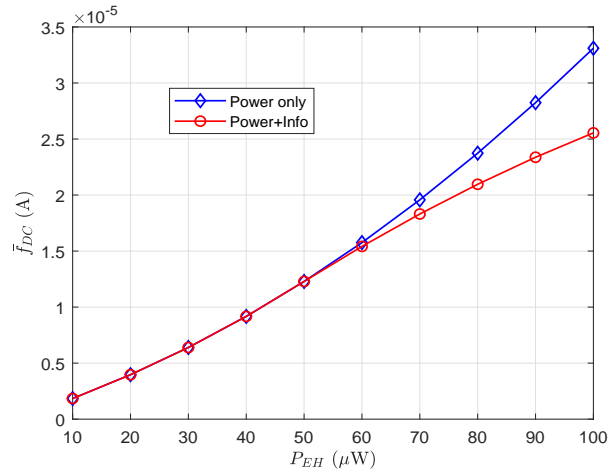
## VII. CONCLUSIONS

The problem of multi-tone optimization for wireless power transmission has been studied in this paper. Two non-linear energy harvester models were discussed: the diode model, and the second-order polynomial curve-fitting model. We showed that the simple second-order polynomial curve-fitting model can be used for formulating the multi-tone optimization problem leading to similar results obtained from the diode non-linear model. This curve-fitting model

(a) Normalized channels frequency response (normalized to  $h_{max}$ ).

(b) Normalized multi-tone amplitudes

Fig. 12. An example for the effect of considering the co-existing information link on power allocation to different tones.

Fig. 13. Average output current represented by  $\bar{f}_{DC}$  vs. normalized transmitted power given by  $P_{EH}$  with and without considering the information link.

can be applied to complicated energy harvester architectures to simplify the formulation of the multi-tone optimization problem. We formulated the multi-tone optimization problem as a linear constrained quadratic program and explained two different solution methods. We provided a global optimal solution for the tones excitation coefficients to maximize the output of the energy harvester. We designed an energy harvester working at 2.4 GHz for evaluating the performance of the curve-fitting model with different allocation strategies using Keysight ADS circuit simulator. Simulation results showed the superiority of our allocation strategy over all existing power allocation strategies. The co-existence of information links with wireless power transmission

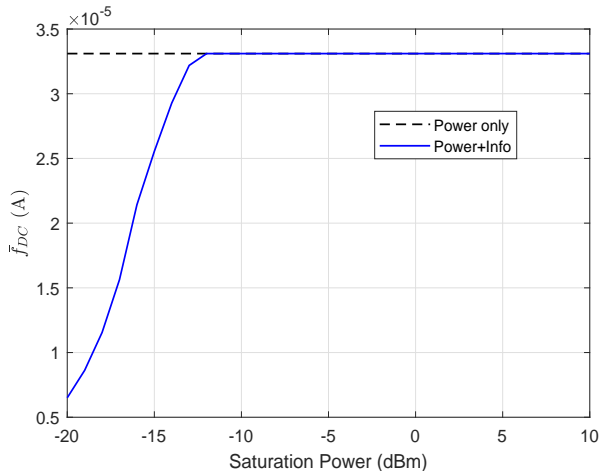
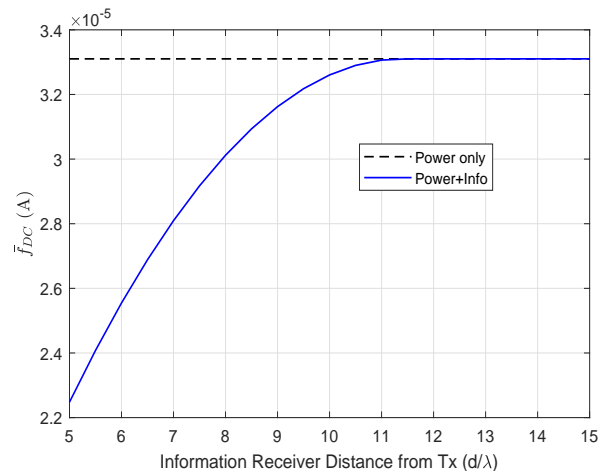
(a)  $\bar{f}_{DC}$  vs. the saturation power of the LNA ( $P_{sat.}$ )(b)  $\bar{f}_{DC}$  vs. the information receiver distance from the power transmitter normalized to the wavelength ( $\frac{d}{\lambda}$ ).

Fig. 14. Study of the average output current represented by  $\bar{f}_{DC}$  vs. saturation power of the LNA and the distance of the information receiver from the power transmitter. The energy harvester is fixed at  $d = 8\lambda$  with  $P_{EH} = 100 \mu\text{W}$ . The dotted black line indicates the average output current without considering the constraint on  $P_{sat.}$

has been studied in this paper by introducing a constraint on the received power at the nearby information receiver, which is operating in the same band as the wireless power transmitter, to prevent its LNA from saturation and producing harmonics interfering with the information signal. Performance evaluations highlighted the importance of considering the saturation power, and the distance of the information receiver from the power transmitter when designing the multi-tone signal. Considering co-location of power and information transmission as well as incorporating non-linear energy harvester models, which are valid in the low-power region, in the areas of wirelessly powered communications and backscatter communications is promising for future research.

#### ACKNOWLEDGMENT

The authors would like to thank Christos I. Kolitsidas for his help in setting up the experiment described in the introduction of this paper and for the fruitful discussions during the early stages of this work.

#### REFERENCES

- [1] K. Huang and X. Zhou, "Cutting the last wires for mobile communications by microwave power transfer," *IEEE Communications Magazine*, vol. 53, no. 6, pp. 86–93, June 2015.
- [2] C. R. Valenta and G. D. Durgin, "Harvesting wireless power: Survey of energy-harvester conversion efficiency in far-field, wireless power transfer systems," *IEEE Microwave Magazine*, vol. 15, no. 4, pp. 108–120, June 2014.

- [3] Cost Action IC1301 Team, "Europe and the future for WPT : European contributions to wireless power transfer technology," *IEEE Microwave Magazine*, vol. 18, no. 4, pp. 56–87, June 2017.
- [4] X. Zhao, V. Sadhu, A. Yang, and D. Pompili, "Improved circuit design of analog joint source channel coding for low-power and low-complexity wireless sensors," *IEEE Sensors Journal*, vol. 18, no. 1, pp. 281–289, Jan 2018.
- [5] S. Bi, C. K. Ho, and R. Zhang, "Wireless powered communication: opportunities and challenges," *IEEE Communications Magazine*, vol. 53, no. 4, pp. 117–125, April 2015.
- [6] I. Krikidis, S. Timotheou, S. Nikolaou, G. Zheng, D. W. K. Ng, and R. Schober, "Simultaneous wireless information and power transfer in modern communication systems," *IEEE Communications Magazine*, vol. 52, no. 11, pp. 104–110, Nov 2014.
- [7] R. Correia and N. B. Carvalho, "Ultrafast backscatter modulator with low-power consumption and wireless power transmission capabilities," *IEEE Microwave and Wireless Components Letters*, vol. 27, no. 12, pp. 1152–1154, Dec 2017.
- [8] K. Huang and E. Larsson, "Simultaneous information and power transfer for broadband wireless systems," *IEEE Transactions on Signal Processing*, vol. 61, no. 23, pp. 5972–5986, Dec 2013.
- [9] R. Zhang and C. K. Ho, "MIMO broadcasting for simultaneous wireless information and power transfer," *IEEE Transactions on Wireless Communications*, vol. 12, no. 5, pp. 1989–2001, May 2013.
- [10] E. Boshkovska, D. W. K. Ng, N. Zlatanov, and R. Schober, "Practical non-linear energy harvesting model and resource allocation for SWIPT systems," *IEEE Communications Letters*, vol. 19, no. 12, pp. 2082–2085, Dec 2015.
- [11] B. Clerckx, "Waveform optimization for SWIPT with nonlinear energy harvester modeling," in *WSA 2016; 20th International ITG Workshop on Smart Antennas*, March 2016, pp. 1–5.
- [12] X. Xu, A. Ozcelikkale, T. McKelvey, and M. Viberg, "Simultaneous information and power transfer under a non-linear RF energy harvesting model," in *2017 IEEE International Conference on Communications Workshops (ICC Workshops)*, May 2017, pp. 179–184.
- [13] G. A. Vera, A. Georgiadis, A. Collado, and S. Via, "Design of a 2.45 GHz rectenna for electromagnetic (EM) energy scavenging," in *2010 IEEE Radio and Wireless Symposium (RWS)*, Jan 2010, pp. 61–64.
- [14] H. Sun, Z. Zhong, and Y. Guo, "An adaptive reconfigurable rectifier for wireless power transmission," *IEEE Microwave and Wireless Components Letters*, vol. 23, no. 9, pp. 492–494, Sept 2013.
- [15] U. Olgun, C. Chen, and J. L. Volakis, "Investigation of rectenna array configurations for enhanced RF power harvesting," *IEEE Antennas and Wireless Propagation Letters*, vol. 10, pp. 262–265, 2011.
- [16] C. Song, Y. Huang, J. Zhou, J. Zhang, S. Yuan, and P. Carter, "A high-efficiency broadband rectenna for ambient wireless energy harvesting," *IEEE Transactions on Antennas and Propagation*, vol. 63, no. 8, pp. 3486–3495, Aug 2015.
- [17] A. Collado and A. Georgiadis, "Optimal waveforms for efficient wireless power transmission," *IEEE Microwave and Wireless Components Letters*, vol. 24, no. 5, pp. 354–356, May 2014.
- [18] C. R. Valenta and G. D. Durgin, "Rectenna performance under power-optimized waveform excitation," in *2013 IEEE International Conference on RFID (RFID)*, April 2013, pp. 237–244.
- [19] M. Rajabi, N. Pan, S. Pollin, and D. Schreurs, "Impact of multisine excitation design on rectifier performance," in *2016 46th European Microwave Conference (EuMC)*, Oct 2016, pp. 1151–1154.
- [20] B. Clerckx and E. Bayguzina, "Waveform design for wireless power transfer," *IEEE Transactions on Signal Processing*, vol. 64, no. 23, pp. 6313–6328, Dec 2016.
- [21] M. R. V. Moghadam, Y. Zeng, and R. Zhang, "Waveform optimization for radio-frequency wireless power transfer," in *2017 IEEE 18th International Workshop on Signal Processing Advances in Wireless Communications (SPAWC)*, July 2017, pp. 1–6.

- [22] S. Lee, Y. Zeng, and R. Zhang, "Retrodirective multi-user wireless power transfer with massive MIMO," *IEEE Wireless Communications Letters*, vol. 7, no. 1, pp. 54–57, Feb 2018.
- [23] G. Yang, C. K. Ho, and Y. L. Guan, "Multi-antenna wireless energy transfer for backscatter communication systems," *IEEE Journal on Selected Areas in Communications*, vol. 33, no. 12, pp. 2974–2987, Dec 2015.
- [24] J. P. Curty, N. Joehl, F. Krummenacher, C. Dehollain, and M. J. Declercq, "A model for  $\mu$ -power rectifier analysis and design," *IEEE Transactions on Circuits and Systems I: Regular Papers*, vol. 52, no. 12, pp. 2771–2779, Dec 2005.
- [25] A. Boaventura, A. Collado, N. B. Carvalho, and A. Georgiadis, "Optimum behavior: Wireless power transmission system design through behavioral models and efficient synthesis techniques," *IEEE Microwave Magazine*, vol. 14, no. 2, pp. 26–35, March 2013.
- [26] A. S. Boaventura and N. B. Carvalho, "Maximizing DC power in energy harvesting circuits using multi-sine excitation," in *2011 IEEE MTT-S International Microwave Symposium*, June 2011, pp. 1–1.
- [27] Y. Chen, N. Zhao, and M. S. Alouini, "Wireless energy harvesting using signals from multiple fading channels," *IEEE Transactions on Communications*, vol. 65, no. 11, pp. 5027–5039, Nov 2017.
- [28] Y. Chen, K. T. Sabnis, and R. A. Abd-Alhameed, "New formula for conversion efficiency of RF EH and its wireless applications," *IEEE Transactions on Vehicular Technology*, vol. 65, no. 11, pp. 9410–9414, Nov 2016.
- [29] S. Burer and D. Vandembussche, "A finite branch-and-bound algorithm for nonconvex quadratic programming via semidefinite relaxations," *Mathematical Programming*, vol. 113, no. 2, pp. 259–282, Jun 2008. [Online]. Available: <https://doi.org/10.1007/s10107-006-0080-6>
- [30] J. Chen and S. Burer, "Globally solving nonconvex quadratic programming problems via completely positive programming," *Mathematical Programming Computation*, vol. 4, no. 1, pp. 33–52, Mar 2012. [Online]. Available: <https://doi.org/10.1007/s12532-011-0033-9>
- [31] W. Xia, J. Vera, and L. F. Zuluaga, "Globally solving non-convex quadratic programs via linear integer programming techniques," *ArXiv e-prints*, Nov. 2015.
- [32] S. Burer and D. Vandembussche, "Globally solving box-constrained nonconvex quadratic programs with semidefinite-based finite branch-and-bound," *Computational Optimization and Applications*, vol. 43, no. 2, pp. 181–195, Jun 2009. [Online]. Available: <https://doi.org/10.1007/s10589-007-9137-6>
- [33] D. Pozar, *Microwave Engineering, 4th Edition*. Wiley, 2011.
- [34] Z. B. Zawawi, J. Park, and B. Clerckx, "Simultaneous wireless information and power transfer in a two-user OFDM interference channel," in *2015 International Symposium on Wireless Communication Systems (ISWCS)*, Aug 2015, pp. 266–270.
- [35] E. A. Jorswieck, E. G. Larsson, and D. Danev, "Complete characterization of the pareto boundary for the MISO interference channel," *IEEE Transactions on Signal Processing*, vol. 56, no. 10, pp. 5292–5296, Oct 2008.
- [36] S. Timotheou, I. Krikidis, G. Zheng, and B. Ottersten, "Beamforming for MISO interference channels with QoS and RF energy transfer," *IEEE Transactions on Wireless Communications*, vol. 13, no. 5, pp. 2646–2658, May 2014.
- [37] B. Clerckx and E. Bayguzina, "Low-complexity adaptive multisine waveform design for wireless power transfer," *IEEE Antennas and Wireless Propagation Letters*, vol. 16, pp. 2207–2210, 2017.